INTERNATIONAL JOURNAL OF ENERGY
DOI: 10.46300/91010.2022.16.8 Volume 16, 2022

Five-level DTC-ANN with balancing strategy of DSIM

Elakhdar Benyoussef, Said Barkat
Department of Electrical Engineering, University of Kasdi Merbah, Ouargla 30000, BP. 511 Algeria

Abstract— This paper presents an artificial neural networks controller devoted to improve the performance of direct torque control strategy of double star induction machine fed by two five-level diode-clamped inverters. The resulting control scheme presents enough degrees of freedom to control both torque and flux with very low ripple and high dynamics. Unfortunately, the diode-clamped inverter has an inherent problem of DC-link capacitors voltages variations. To overcome this problem, an artificial neural network based direct torque control with balancing strategy is proposed to suppress the unbalance of DC-link capacitor voltages. Simulations results are given to show the effectiveness and the robustness of the suggested control method.

Keywords— Double Star Induction Machine; Five-Level Diode Clamped Inverter; Balancing Strategy; Direct Torque Control; Artificial Neural Networks Control.

I. INTRODUCTION

THE multiphase drive systems have numerous advantages over conventional three-phase drives such as reduced rotor harmonic currents, reduced torque pulsations, magnetic flux harmonic reduction, and lower current per phase without increasing the voltage per phase and higher torque per RMS ampere for the same machine volume [1, 2].

Five-phase and six-phase induction or synchronous machines are the common multiphase machines [3]. These types of machines drives are widely used in several applications especially in the field of high power electrical/hybrid, rolling stock traction systems such as locomotive and electric ship propulsion [4]. Recently, special attention is given to the double star machine drive systems [5]. Normally two two-level inverters are indispensable for double star electrical drive. So, in the field of high power drive systems, the level of DC-bus voltage constitutes an important limitation on the handled power.

In this context, multilevel inverters have been used for power conversion in high-power applications such as utility and large motor drive applications. In a multilevel inverter, a desired output voltage waveform can be synthesized from multiple voltage levels with less distortion, less switching frequency, higher efficiency, and lower voltage devices. Compared to conventional two-level converters, multilevel converters show great advantages such as high power quality of waveforms, low switching losses, high-voltage capability, and low electromagnetic interference [6]. In general, multilevel converters can be categories into three types: diode-clamped multilevel converters, flying capacitor multilevel converters, and cascaded multilevel converters with separated DC sources [7].

Among these inverter topologies, multilevel diode-clamped inverter (DCI) reaches the higher output voltage and power levels and the higher reliability due to its modular topology [8]. However, the unbalance of the input DC voltages of the diode-clamped multilevel topology constitutes the major limitation facing the use of this power converter. To balance the voltage of DC-link series capacitors, three main approaches have been proposed, which are: using separate DC sources, adding some auxiliary balancing circuits, and using space vector modulation technique by selecting redundant switching states [9].

On the other hand, the multilevel direct torque control (DTC) of electrical drives has become an attracting topic in research and academic community over the past decade [10]. This control is based on the decoupled control of flux and torque providing a very quick and robust response with a simple control approach [11]. The main advantages of DTC are the absence of coordinate transformation, there is no need for current regulators, and the absence of separate voltage modulation block. However, the significant disadvantage of conventional DTC is ripples, which exist in the torque and flux variables. In the aim to improve the performance of the electrical drives based on DTC, neural network direct torque control (DTC-ANN) attracts more and more the attention of many researches [12].

The objective of this paper is to propose a multilevel DTC based on artificial neural network method with efficient DC-voltages balancing control method dedicates to double star induction machine.

The present paper structure is as follows: in Section II, the DTC-ANN with voltage balancing strategy principal is presented. In Section III, the model of the DSIM is presented; a suitable transformation matrix is used to develop a simple dynamic model. The proposed five-level is briefly presented in Section IV. Section V is reserved to DC capacitor voltages balancing analysis. In Section VI, the DTC strategy is applied to get decoupled control of the flux and torque. In order to improve the static and dynamic control performance of the DSIM, the switching tables used in DTC are substituted by an artificial neural network controller in Section VII. In Section VIII, a comparative study between two-level DTC-ANN and five-level DTC-ANN with balancing strategy is presented.

INTERNATIONAL JOURNAL OF ENERGY
DOI: 10.46300/91010.2022.16.8 Volume 16, 2022

I. PRINCIPAL OF THE DTC-ANN USING VOLTAGE BALANCING STRATEGY

The general structure of the double star induction machine fed by two five-level inverters and controlled by DTC-ANN is represented in Fig 1. It includes closed loop control of speed using PI controller.

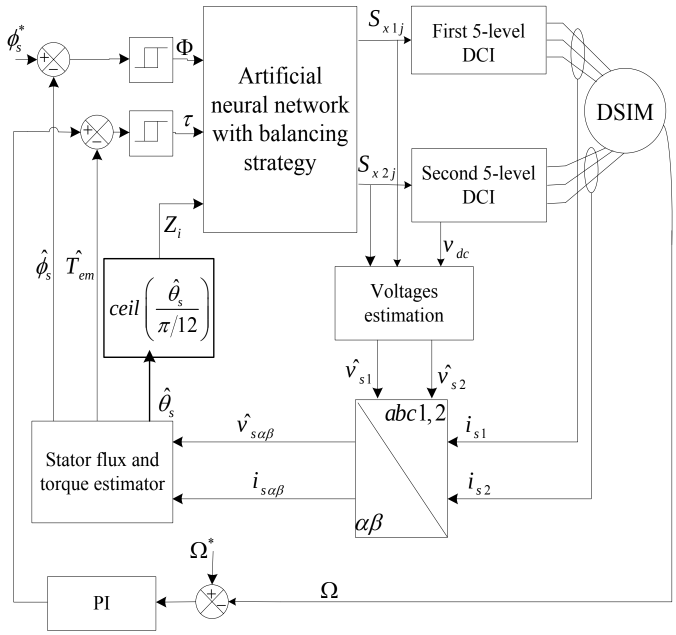

Fig. 1 Five-level DTC-ANN scheme with balancing strategy (j=*1*, 2, …. , *12*).

II. MODELING OF THE DOUBLE STAR INDUCTION MACHINE

A schematic of the stator and rotor windings for a double star induction machine is given in Fig 2.

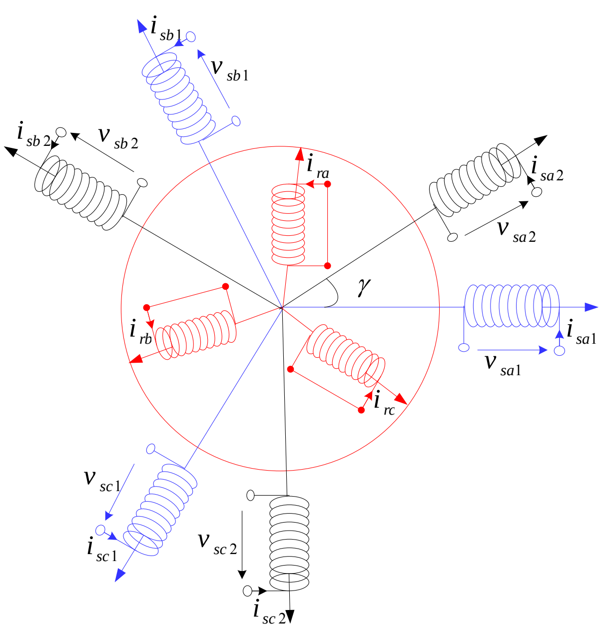

Fig. 2 DSIM windings representation.

The machine model is established based on the following assumptions: the air gap is uniform, the windings are sinusoidally distributed around the air gap, and the magnetic saturation as well as core losses are neglected. The DSIM has two sets of three-phase windings spatially shifted by $\gamma = 30$ electrical degrees with isolated neutral points [13].

The voltage equations in the original phase coordinates can be expressed as:

$$\begin{cases} v_{s1} = R_s i_{s1} + \dfrac{d\phi_{s1}}{dt} \\ v_{s2} = R_s i_{s2} + \dfrac{d\phi_{s2}}{dt} \\ 0 = R_r i_r + \dfrac{d\phi_r}{dt} \end{cases} \qquad (1)$$

with

$v_{s1} = [v_{sa1} \quad v_{sb1} \quad v_{sc1}]^T$:Stator voltages of the first winding;

$v_{s2} = [v_{sa2} \quad v_{sb2} \quad v_{sc2}]^T$: Stator voltages of the second winding;

$i_{s1} = [i_{sa1} \quad i_{sb1} \quad i_{sc1}]^T$: Stator currents of the first winding;

$i_{s2} = [i_{sa2} \quad i_{sb2} \quad i_{sc2}]^T$: Stator currents of the second winding;

$i_r = [i_{ra} \quad i_{rb} \quad i_{rc}]^T$: Rotor currents;

$\phi_{s1} = [\phi_{sa1} \quad \phi_{sb1} \quad \phi_{sc1}]^T$: Stator flux of the first winding;

$\phi_{s2} = [\phi_{sa2} \quad \phi_{sb2} \quad \phi_{sc2}]^T$: Stator flux of the second winding;

$\phi_r = [\phi_{ra} \quad \phi_{rb} \quad \phi_{rc}]^T$: Rotor flux;

$R_s = Diag\left[R_s \quad R_s \quad R_s\right]$: Diagonal 3×3 stator and rotor resistance matrix.

The original six-dimensional stator system can be decomposed into three two-dimensional decoupled subsystems (α,β), (z_1,z_2) and (z_3,z_4), using the following transformation:

$$\left[X_{s\alpha} \quad X_{s\beta} \quad X_{z1} \quad X_{z2} \quad X_{z3} \quad X_{z4}\right]^T = \left[A\right]\left[X_s\right]^T \qquad (2)$$

with $\left[X_s\right] = \left[X_{s1} \quad X_{s2}\right]$

where X_s can refer to stator currents vector (i_s), stator flux vector (ϕ_s), or stator voltages vector (v_s).

The matrix A is given by:

$$[A] = \frac{1}{\sqrt{3}} \begin{bmatrix} \cos(0) & \cos\left(\frac{2\pi}{3}\right) & \cos\left(\frac{4\pi}{3}\right) & \cos(\gamma) & \cos\left(\frac{2\pi}{3}+\gamma\right) & \cos\left(\frac{4\pi}{3}+\gamma\right) \\ \sin(0) & \sin\left(\frac{2\pi}{3}\right) & \sin\left(\frac{4\pi}{3}\right) & \sin(\gamma) & \sin\left(\frac{2\pi}{3}+\gamma\right) & \sin\left(\frac{4\pi}{3}+\gamma\right) \\ \cos(0) & \cos\left(\frac{4\pi}{3}\right) & \cos\left(\frac{2\pi}{3}\right) & \cos(\pi-\gamma) & \cos\left(\frac{\pi}{3}-\gamma\right) & \cos\left(\frac{5\pi}{3}-\gamma\right) \\ \sin(0) & \sin\left(\frac{4\pi}{3}\right) & \sin\left(\frac{2\pi}{3}\right) & \sin(\pi-\gamma) & \sin\left(\frac{\pi}{3}-\gamma\right) & \sin\left(\frac{5\pi}{3}-\gamma\right) \\ 1 & 1 & 1 & 0 & 0 & 0 \\ 0 & 0 & 0 & 1 & 1 & 1 \end{bmatrix} \qquad (3)$$

II.1. Electrical equations in α-β reference frame

The stator and rotor voltage equations of DSIM in stationary frame are given by:

$$\begin{cases} v_{s\alpha} = R_s i_{s\alpha} + \dfrac{d\phi_{s\alpha}}{dt} \\ v_{s\beta} = R_s i_{s\beta} + \dfrac{d\phi_{s\beta}}{dt} \\ 0 = R_r i_{r\alpha} + \dfrac{d\phi_{r\alpha}}{dt} + p\Omega\phi_{r\beta} \\ 0 = R_r i_{r\beta} + \dfrac{d\phi_{r\beta}}{dt} - p\Omega\phi_{r\alpha} \end{cases} \tag{4}$$

The stator and rotor flux linkages in the same frame:

$$\begin{cases} \phi_{s\alpha} = L_s i_{s\alpha} + M i_{r\alpha} \\ \phi_{s\beta} = L_s i_{s\beta} + M i_{r\beta} \\ \phi_{r\alpha} = L_r i_{r\alpha} + M i_{s\alpha} \\ \phi_{r\beta} = L_r i_{r\beta} + M i_{s\beta} \end{cases} \tag{5}$$

with:

$v_{s\alpha}$, $v_{s\beta}$: The α-β components of stator voltage;

$i_{s\alpha}$, $i_{s\beta}$: The α-β components of stator current;

$i_{r\alpha}$, $i_{r\beta}$: The α-β components of rotor current;

$\phi_{s\alpha}$, $\phi_{s\beta}$: The α-β components of stator flux;

$\phi_{r\alpha}$, $\phi_{r\beta}$: The α-β components of rotor flux.

II.2. Electrical equations in z_1, z_2, z_3, z_4 reference frame

In such frame, the stator voltages equations are given by:

$$\begin{bmatrix} v_{z1} \\ v_{z2} \\ v_{z3} \\ v_{z4} \end{bmatrix} = R_s \begin{bmatrix} i_{z1} \\ i_{z2} \\ i_{z3} \\ i_{z4} \end{bmatrix} + \begin{bmatrix} l_s & 0 & 0 & 0 \\ 0 & l_s & 0 & 0 \\ 0 & 0 & l_s & 0 \\ 0 & 0 & 0 & l_s \end{bmatrix} \frac{d}{dt} \begin{bmatrix} i_{z1} \\ i_{z2} \\ i_{z3} \\ i_{z4} \end{bmatrix} \tag{6}$$

where $L_s = l_s + M$ and $L_r = l_r + M$.

L_s, L_r : Stator and rotor inductance respectively;

l_s, l_r : Stator and rotor leakage inductance respectively;

M : Mutual inductance between stator and rotor.

The harmonic currents i_{z1} and i_{z2} must be as low as possible to reduce the extra losses in the DSIM. These currents are only limited by stator resistance and leakage inductance.

The currents i_{z3} and i_{z4} are equal to zero because the two three-phase windings are connected with isolated neutrals.

The mechanical equation is given by:

$$J\frac{d\Omega}{dt} = T_{em} - T_L - f\Omega \tag{7}$$

With:

T_{em} : Electromagnetic torque;

T_L : Load torque;

Ω : Rotor speed;

f : Friction coefficient;

J : Rotor moment of inertia.

The electromagnetic torque is given by:

$$T_{em} = p\left(\phi_{s\alpha} i_{s\beta} - \phi_{s\beta} i_{s\alpha}\right) \tag{8}$$

III. Modeling of the Five-Level Inverter

Fig 3 shows a three-phase five-level diode-clamped inverter. The order of switches numbering for first phase is $(S_{ak1},..., S_{ak8})$ and likewise for other two phases. The DC-bus consists of four capacitors acting as voltage divider. For a DC-bus voltage v_{dc}, the voltage across each capacitor is $v_{dc}/4$ and voltage stress on each device is limited to v_{dc} through clamping diode [14].

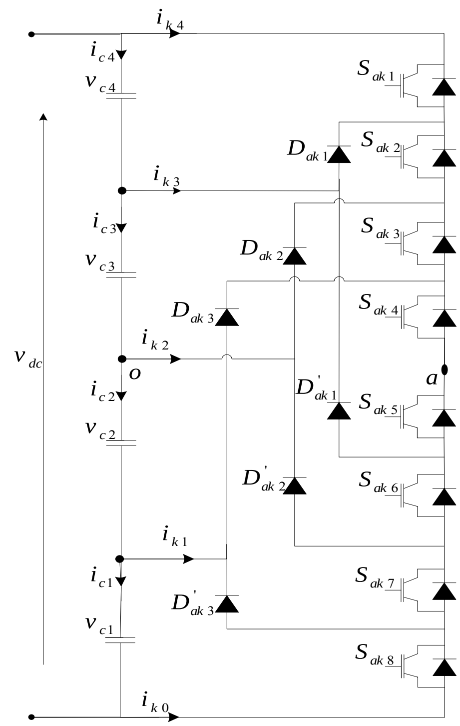

Fig. 3 One phase-leg for a five-level DCI Inverter (k=1 for first inverter and k=2 for second inverter).

Table 1 shows the output voltage levels and the corresponding switch states of the chosen five-level DCI. The switches are arranged into four pairs. If one switch of the pair is turned ON, the complementary switch of the same pair must be OFF. Four switches are triggered at any point of time to select the desired level in the five-level DCI.

State	S_{xk1}	S_{xk2}	S_{xk3}	S_{xk4}	S_{xk5}	S_{xk6}	S_{xk7}	S_{xk8}	v_{xko}
4	1	1	1	1	0	0	0	0	$v_{c3}+v_{c4}$
3	0	1	1	1	1	0	0	0	v_{c3}
2	0	0	1	1	1	1	0	0	0
1	0	0	0	1	1	1	1	0	$-v_{c2}$
0	0	0	0	0	1	1	1	1	$-(v_{c1}+v_{c2})$

Table 1 Switching states of five-level DCI ($i = 1…8$, $k = 1, 2$, x=*a*, *b* or *c*).

The boolean function F_{xki} associated to the switch S_{xki} is defined by:

$$F_{xki}=\begin{cases}1 & S_{xki} \quad is \quad ON\\ 0 & S_{xki} \quad is \quad OFF\end{cases} \tag{9}$$

For each leg of the inverter, five connections functions can be defined as:

$$\begin{cases}F_{cxk1}=F_{xk1}F_{xk2}F_{xk3}F_{xk4}\\ F_{cxk2}=F_{xk2}F_{xk3}F_{xk4}F_{xk5}\\ F_{cxk3}=F_{xk3}F_{xk4}F_{xk5}F_{xk6}\\ F_{cxk4}=F_{xk4}F_{xk5}F_{xk6}F_{xk7}\\ F_{cxk5}=F_{xk5}F_{xk6}F_{xk7}F_{xk8}\end{cases} \tag{10}$$

Finally, the phase voltages v_{sak}, v_{sbk}, v_{sck} of each inverter can be written as:

$$\begin{bmatrix}v_{sak}\\ v_{sbk}\\ v_{sck}\end{bmatrix}=\begin{bmatrix}F_{cak1} & F_{cak2} & F_{cak3} & F_{cak4} & F_{cak5}\\ F_{cbk1} & F_{cbk2} & F_{cbk3} & F_{cbk4} & F_{cbk5}\\ F_{cck1} & F_{cck2} & F_{cck3} & F_{cck4} & F_{cck5}\end{bmatrix}\begin{bmatrix}v_{c3}+v_{c4}\\ v_{c3}\\ 0\\ -v_{c2}\\ -(v_{c1}+v_{c2})\end{bmatrix} \tag{11}$$

IV. DC-Capacitor Voltage Balancing Strategy

The capacitor voltage balancing strategy proposed in this work is based on minimum energy property. By selecting an appropriate redundant switching state that minimizes a specific cost function, drift voltage phenomenon of DC capacitors voltage can be controlled [16].

In a five-level DCI, the total energy E of four capacitors is:

$$E_k=\frac{1}{2}\sum_{j=1}^{4}C_j v_{cj} \tag{12}$$

Where

$$\sum_{j=1}^{4}\left(v_{cj}-v_{dc}\right)=0 \tag{13}$$

By making a change of variable from v_{cj} to $(v_{cj}-v_{dc})/4$ in (11) the positive definite cost function becomes:

$$J=\frac{1}{2}C\sum_{j=1}^{4}\Delta v_{cj}^{2} \tag{14}$$

where:

$$\Delta v_{cj}=v_{cj}-v_{dc}/4 \tag{15}$$

A control method should minimize (12) to achieve voltage balancing [17]. Indeed, based on a proper selection of redundant vectors, J can be minimized if the capacitor voltages are maintained at voltage reference values of $(v_{dc}/4)$.

The mathematical condition to minimize J is:

$$\frac{dJ}{dt}=C\sum_{j=1}^{4}\Delta v_{cj}\frac{dv_{cj}}{dt}=\sum_{j=1}^{4}\Delta v_{cj}i_{cj} \tag{16}$$

with:
Δv_{cj} : The voltage deviation of capacitor C_j ;
i_{ckj} : The current through capacitor C_j .

The capacitor currents i_{ckj} in (16) are affected by the DC-side intermediate branch currents i_{k3}, i_{k2} and i_{k1}, which can be calculated if the switching states used in the switching pattern are known. Thus, it is advantageous to express (16) in terms of i_{k3}, i_{k2} and i_{k1}.

The DC-capacitor currents are expressed as:

$$i_{cj}=\frac{1}{4}\sum_{y=1}^{3}y\left(\sum_{k=1}^{2}i_{ky}\right)-\sum_{y=j}^{3}\left(\sum_{k=1}^{2}i_{ky}\right) \tag{17}$$

By substituting i_{ckj} calculated from (17) in (16), the condition to achieve voltage balancing is deduced as:

$$\sum_{j=1}^{4}\Delta v_{cj}\left(\frac{1}{4}\sum_{y=1}^{3}y\left(\sum_{k=1}^{2}i_{ky}\right)-\sum_{y=j}^{3}\left(\sum_{k=1}^{2}i_{ky}\right)\right)\le 0 \tag{18}$$

Since the net DC-link voltage is regulated at v_{dc}

$$\sum_{j=1}^{4}\Delta v_{cj}=0 \tag{19}$$

Substituting Δv_{c4}, calculated from (19), in (18) it yields

$$\sum_{j=1}^{3}\Delta v_{cj}\left(\sum_{y=j}^{3}\left(\sum_{k=1}^{2}i_{ky}\right)\right) \tag{20}$$

By applying the averaging operator, over one sampling period, to (20), it results:

$$\frac{1}{T}\sum_{KT}^{(K+1)T}\Delta v_{cj}\left(\sum_{y=j}^{3}\left(\sum_{k=1}^{2}i_{ky}\right)\right)dt \geq 0 \tag{21}$$

Equation (20) can be simplified to:

$$\sum_{j=1}^{3}\Delta v_{cj}(K)\left(\sum_{y=j}^{3}\left(\sum_{k=1}^{2}\bar{i}_{ky}\right)(K)\right)dt \geq 0 \tag{22}$$

where:

$\Delta v_{cj}(K)$: The voltage drifts of C_j at sampling period K.

$\bar{i}_{ky}(K)$: The averaged value of the j^{th} DC-side intermediate branch current.

For the five-level FLDTC balancing strategy the cost function is given by:

$$J_K = \sum_{j=1}^{3}\Delta v_{cj}(K)\left(\sum_{y=j}^{3}\left(\sum_{k=1}^{2}\bar{i}_{ky}(K)\right)\right) \tag{23}$$

To calculate $\bar{i}_{ky}$ ($y=1,...,3$), contributions of switching states to the DC side intermediate branch currents and relationship between the DC and AC side currents, i_{ka}, i_{kb}, and i_{kc}, are required.

$$\begin{cases} i_{k3} = F_{Cak3}i_{ak} + F_{Cbk3}i_{bk} + F_{Cck3}i_{ck} \\ i_{k2} = F_{Cak2}i_{ak} + F_{Cbk2}i_{bk} + F_{Cck2}i_{ck} \\ i_{k1} = F_{Cak1}i_{ak} + F_{Cbk1}i_{bk} + F_{Cck1}i_{ck} \end{cases} \tag{24}$$

The currents $\bar{i}_{ky}$ are calculated based on (24) for each set of switching combinations; they are replaced in (23) and the best set that fulfills the condition is selected.

For example the switching states in sector I that are adjacent to the triangle are (421, 310), (411, 300) and (410) using equation (23) one obtained the Table 2.

i_{ky}	421	310	411	300	410
i_{k1}	i_{ck}	i_{bk}	$-i_{ak}$	0	i_{bk}
i_{k2}	i_{bk}	0	0	0	0
i_{k3}	0	i_{ak}	0	i_{ak}	0

Table 2. Example for switching states in first sector

Fig. 4 shows a schematic diagram of the five-level DTC-ANN balancing system including the DC capacitor voltage control strategy.

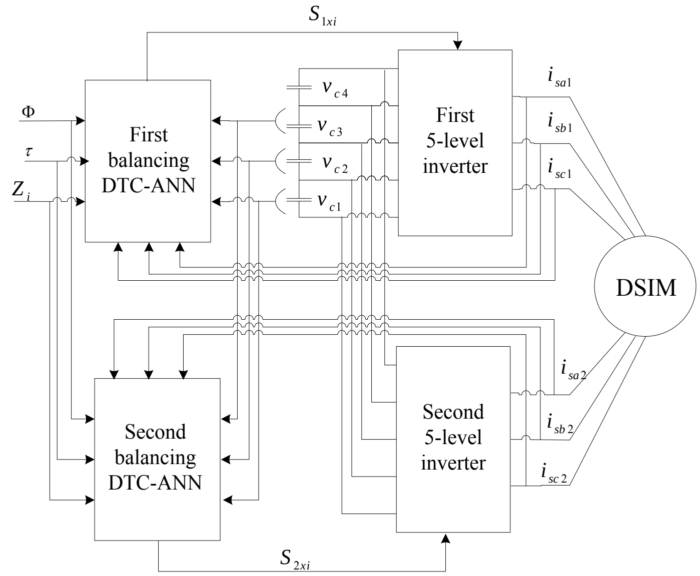

Fig. 4 Schematic representation of the five-level DTC-ANN with balancing strategy

V. Conventional Direct Torque Control Strategy

Direct torque control consists of choosing a voltage vector based on a switching table according to the flux and torque errors as well as the stator flux vector position. In this technique, the rotor position is no longer needed [10].

The stator voltage estimator can be obtained by the following equation:

$$\begin{bmatrix}\hat{v}_{s\alpha}\\ \hat{v}_{s\beta}\end{bmatrix} = [A]\begin{bmatrix}\hat{v}_{s1}\\ \hat{v}_{s2}\end{bmatrix} \tag{25}$$

The expression of the stator flux components is written as:

$$\begin{cases} \hat{\phi}_{s\alpha} = \int_0^t \left(v_{s\alpha} - R_s i_{s\alpha}\right)d\tau + \hat{\phi}_{s\alpha}(0) \\ \hat{\phi}_{s\beta} = \int_0^t \left(v_{s\beta} - R_s i_{s\beta}\right)d\tau + \hat{\phi}_{s\beta}(0) \end{cases} \tag{26}$$

The magnitude of stator flux and their angle are estimated by:

$$\begin{cases} \left|\hat{\phi}_s\right| = \sqrt{\hat{\phi}_{s\alpha}^2 + \hat{\phi}_{s\beta}^2} \\ \hat{\theta}_s = \tan\left(\dfrac{\hat{\phi}_{s\beta}}{\hat{\phi}_{s\alpha}}\right)^{-1} \end{cases} \tag{27}$$

Fig. 5 illustrates the switching states of a five-level diode-clamped inverter. Since five kinds of switching states exist in each phase, the five-level inverter has 125 switching states and there are 61 effective vectors. According to the magnitude of the voltage vectors, the five-level DCI is divides into nine groups [9].

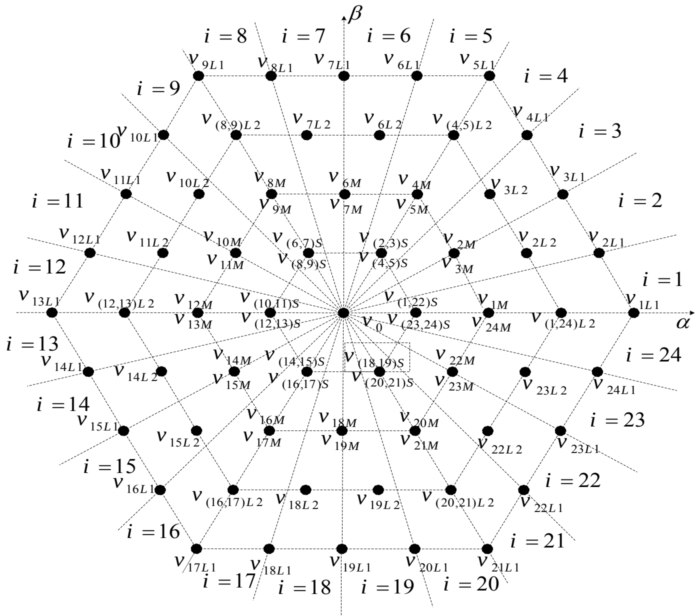

Fig. 5 Switching states of the five-level DCI.

The output voltage vectors, which are selected to change the torque angle are presented in Tables 3 and 4.

Φ	τ	Z_i	Φ	τ	Z_i	Φ	τ	Z_i
	4	$v_{(i+4)L1}$		4	$v_{(i+6)L1}$		4	$v_{(i+8)L1}$
	3	$v_{(i+4)L2}$		3	$v_{(i+6)L2}$		3	$v_{(i+8)L2}$
	2	$v_{(i+4)M}$		2	$v_{(i+6)M}$		2	$v_{(i+8)M}$
	1	$v_{(i+4)S}$		1	$v_{(i+6)S}$		1	$v_{(i+8)S}$
1	0	v_0	0	0	v_0	-1	0	v_0
	-1	$v_{(i+20)S}$		-1	$v_{(i+18)S}$		-1	$v_{(i+16)S}$
	-2	$v_{(i+20)M}$		-2	$v_{(i+18)M}$		-2	$v_{(i+16)M}$
	-3	$v_{(i+20)L2}$		-3	$v_{(i+18)L2}$		-3	$v_{(i+16)L2}$
	-4	$v_{(i+20)L1}$		-4	$v_{(i+18)L1}$		-4	$v_{(i+16)L1}$

Table 3 Switching table used in the conventional DTC of first star for the DSIM.

Φ	τ	Z_i	Φ	τ	Z_i	Φ	τ	Z_i
	4	$v_{(i+2)L1}$		4	$v_{(i+4)L1}$		4	$v_{(i+6)L1}$
	3	$v_{(i+2)L2}$		3	$v_{(i+4)L2}$		3	$v_{(i+6)L2}$
	2	$v_{(i+2)M}$		2	$v_{(i+4)M}$		2	$v_{(i+6)M}$
	1	$v_{(i+2)S}$		1	$v_{(i+4)S}$		1	$v_{(i+6)S}$
1	0	v_0	0	0	v_0	-1	0	v_0
	-1	$v_{(i+18)S}$		-1	$v_{(i+16)S}$		-1	$v_{(i+14)S}$
	-2	$v_{(i+18)M}$		-2	$v_{(i+16)M}$		-2	$v_{(i+14)M}$
	-3	$v_{(i+18)L2}$		-3	$v_{(i+16)L2}$		-3	$v_{(i+14)L2}$
	-4	$v_{(i+18)L1}$		-4	$v_{(i+16)L1}$		-4	$v_{(i+14)L1}$

Table 4 Switching table used in the conventional DTC of second star for the DSIM.

VI. DTC Based on Artificial Neural Networks Strategy

Artificial neural networks use a dense interconnection of computing nodes to approximate nonlinear functions. Each node constitutes a neuron and performs the multiplication of its input signals by constant weights, sums up the results and maps the sum to a nonlinear activation function*;* the result is then transferred to its output. The feed-forward topology shown in the network offers the advantage of simplicity and ease programming. Such a neural network contains three layers: input layer, hidden layers and output layer [15].

The structure of the neural network adopted to perform the DTC of DSIM supplied by two five-level inverters is shown in Fig. 6.

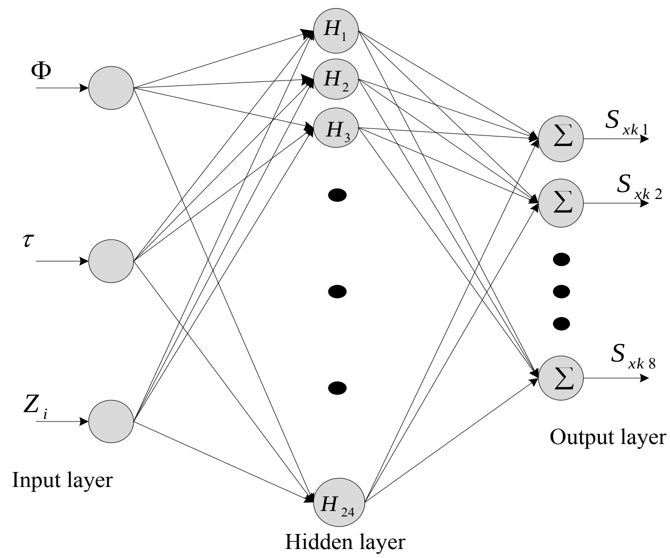

Fig. 6 Neural network structure for five-level DTC.

VII. Comparative Study Between Two-level DTC and Five-Level DTC-ANN

To verify the validity of the proposed controller, the system was simulated using the DSIM parameters given in Appendix. The simulation results are obtained using the following DC-link capacitors values $C_1= C_2= C_3= C_4= 1mF$. The DC side of the inverter is supplied by a constant DC source $v_{dc}=600V$.

The obtained two-level DTC-ANN results are presented and compared with those obtained by five-level DTC-ANN with balancing strategy. The control system was tested under deferent operating conditions such as sudden change of load torque and step change in reference speed.

The DSIM is accelerating from standstill to reference speed *100* rad/s. The system is started with full load torque ($T_L=10$ N.m). Afterwards, a step variation on the load torque ($T_L=0$ N.m) is applied at time $t=0.5$s. And then a sudden reversion in the speed command from *100* rad/s to *-100* rad/s was introduced at *1*s. Indeed, Figs. 6 and 7 show the simulation results obtained for the two-level DTC-ANN and the five-level DTC-ANN with balancing strategy of DSIM, respectively.

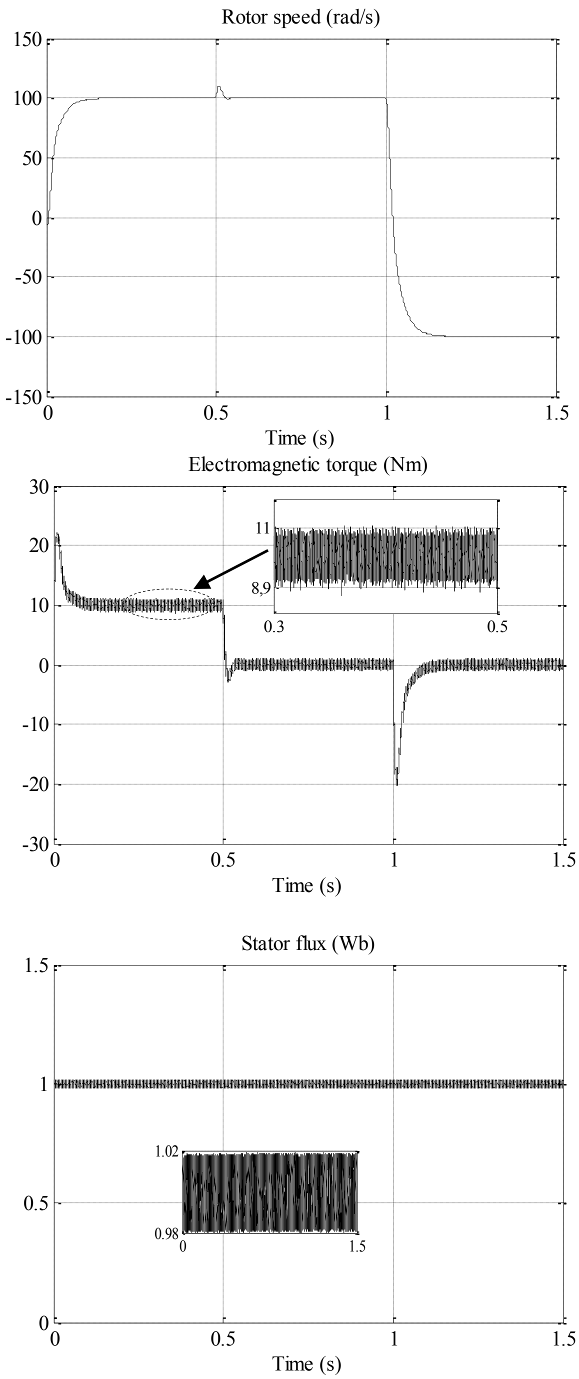

Fig. 7 Dynamic responses of two-level DTC-ANN for DSIM.

Note that the speed follows its reference value while the electromagnetic torque reaches slowly its reference value. Elimination of the load torque causes a slight variation in speed response. The speed controller intervenes to face this variation and ensures that the system follows its suitable reference speed. Moreover, the decoupling control between electromagnetic torque and stator flux is always confirmed. It is important to notice in Fig. 7 that the electromagnetic torque and stator flux ripples are considerably decreased in comparison with Fig. 8.

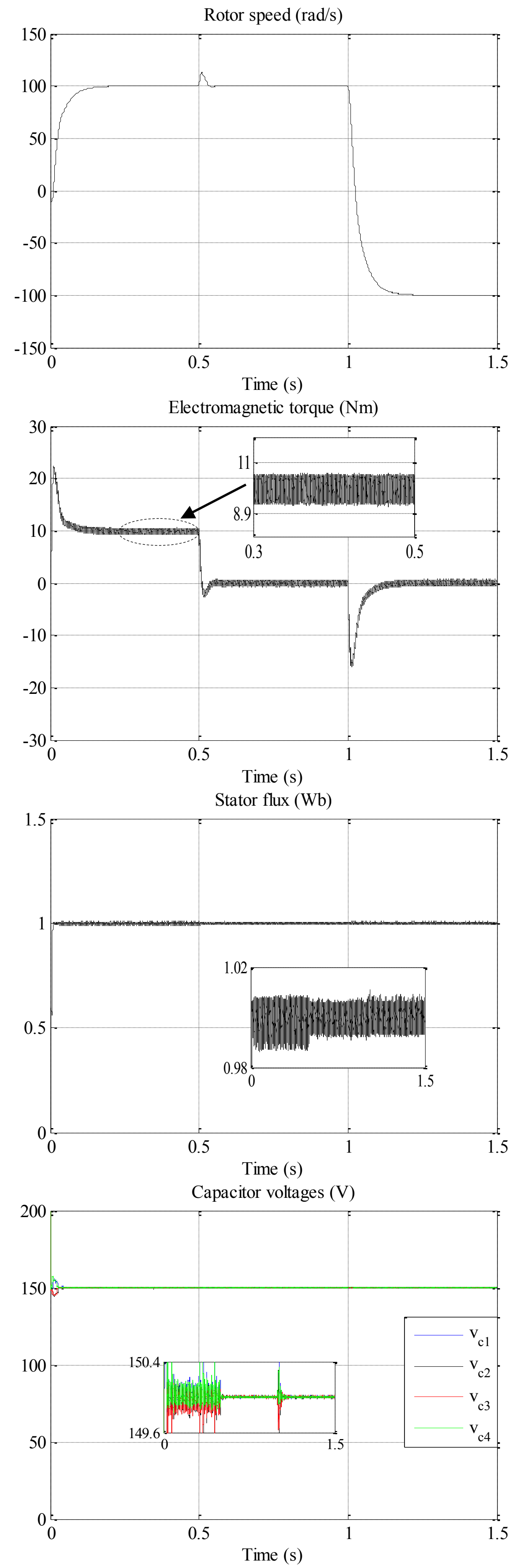

Fig. 8 Dynamic responses of five-level DTC-ANN with balancing strategy for DSIM.

It can be observed also that the proposed balancing strategy is able to guarantee capacitor voltages balance even during the abovementioned transits. In addition, the tracking capability is further improved. Moreover, the decoupling control between torque and stator flux is always confirmed.

VIII. Conclusion

In this paper, a five-level DTC-ANN method applied on DSIM is presented and its merits over the conventional DTC approach are confirmed by simulation results. One important problem with the five-level DCI topology is the problem of voltage imbalance in DC capacitors. The multilevel diode-clamped inverter has an inherent problem of DC-link capacitors voltages fluctuations. This problem can be solved in satisfactory way by using a simplified multilevel DTC-ANN algorithm equipped by a balancing strategy. This solution has offered the opportunity to equalize the different input DC voltages of the inverter and improve the performances of the multiphase machine.

Appendix

The parameters of DSIM are given in Table 5.

Quantity	Symbols	Value
Stator resistance	R_s	4.67 Ω
Rotor resistance	R_r	8 Ω
Stator inductance	L_s	0.374 *H*
Rotor inductance	L_r	0.374 *H*
Mutual inductance	M	0.365 *H*
Inertia moment	J	0.003 kgm^2
Pair of poles	p	1
Rated speed	Ω_n	2830 *rpm*
Rated voltage	v_n	220 *V*
Rated power	P_n	1 *kW*

Table 5. DSIM parameters.

References

[1] L. Schreier, J. Bendl, and M. Chomat, “Analysis of influence of third spatial harmonic on currents and torque of multi-phase synchronous machine with permanent magnets,” Electrical Engineering, vol. 100, no. 3, pp. 2095–2102, 2018.
[2] W. Canders and H. Mosebach, “Multiphase machines with individual slot activation,” Electrical Engineering, vol. 100, pp. 2287–2297, no.4, 2018.
[3] S. Hang, S. Aymen, D. Obrad, and L. Emil, “Parameter estimation of asymmetrical six-phase induction machines using modified standard tests, ” IEEE Transaction on Industrial Electronics, vol. 64, no. 8, 2017.
[4] J. Tiago, N. Nguyen, S. Eric, M. Fabien, and G. Mael, “Dual-multiphase motor drives for fault-tolerant applications: power electronic structure and control strategies,” IEEE Transaction on Power Electronics, vol. 33, no. 1, pp. 572–580, 2018.
[5] G. Alejandro, B. Fernando, J. Malvar, A. Vidal, P. Diego, L. Oscar, and D. Jesus, “Selection criteria of multiphase induction machines for speed sensorless drives based on rotor slot harmonics,” IEEE Transaction on Industrial Electronics, vol. 63, no. 8, 2016.
[6] P. Rajasekaran and V. Jawahar, “Comparison of various strategies in DTFC based multilevel NPC inverter fed induction drive for torque ripple reduction,” Transactions on Electrical and Electronic Materials, vol. 19, no.4, pp. 290–303, 2018.
[7] K. Gayathri, S. Arun, and C. Sreeja, “Comparative study on different five level inverter topologies,” Electrical Power and Energy Systems, vol. 63, pp. 363–372, 2014.
[8] Z. Huaitian, R. Harith, J. Long, L. Jinke, P. Josep, and K. Georgios, “Circulating current control scheme of modular multilevel converters supplying passive networks under unbalanced load conditions,” Electric Power Systems Research, vol. 171, pp. 36–46, 2019.
[9] S. Shunji, W. Xiangzhou, Z. Shuhua, Z. Yanxi, and L. Dongyuan, “A new diode-clamped multilevel inverter with balance voltages of DC capacitors,” IEEE Transaction on Energy Conversion, vol. 33, no. 4, 2018.
[10] S. Ardakani, M. Hosseinpour, M. Shahparasti, and M. Siahi, “Direct torque control of low-voltage three-phase induction motor using three-level eight-switch inverter,” Electrical Engineering, 2019, pp. 1–11.
[11] W. Zheng, W. Xueqing, C. Jiawei, C. Ming, and H. Yihua, “Direct torque control of T-NPC inverters-fed double-stator-winding PMSM drives with SVM,” IEEE Transaction on Power Electronics, vol. 33, no. 2, 2018.
[12] M. Wlas, Z. Krzeminski, J. Guzinski, H. Aburub, and H. Toliyat, “Artificial-neural-network-based sensorless nonlinear control of induction motors,” IEEE Transaction on Energy Conversion, vol. 20, no. 3, 2005.
[13] Z. Tir and Y. Soufi, “Fuzzy logic field oriented control of double star induction motor drive,” Springer of Electrical Engineering, vol. 99, no. 2, pp. 495–503, 2017.
[14] S. Nunsavath, S. Peddapalli, and K. Sushil, “Generalized Algorithm of Reverse Mapping Based SVPWM Strategy for Diode-Clamped Multilevel Inverters,” IEEE Transaction on Industry Application, vol. 54, no. 3, pp. 2425–2437, 2018.
[15] F. Yue and C. Tianyou, “Neural-network-based nonlinear adaptive dynamic decoupling control,” IEEE Transaction on Neural Network, vol. 18, no. 3, pp. 921–925, 2007.
[16] C. Dongdong and G. Qiongxuan, “A novel hybrid voltage balance method for five-level diode-clamped converters,” IEEE Transaction on Industrial Electronics, vol. 65, no. 8, pp. 6020–6031, 2018.
[17] P. Zhiguo, Z. Fang, and K. Corzine, “Voltage balancing control of diode-clamped multilevel rectifier/inverter system,” IEEE Transaction on Industry Applications, vol. 41, no. 6, pp. 1698–1706, 2005.